A Critique of the Triangle Method and a Version Suitable for Estimating Soil Moisture from Satellite Imagery

Toby N. Carlson [a++*]

[a] *Pennsylvania State University, University Park, PA 16802, United States of America.*

Author's contribution

The sole author designed, analyzed, interpreted and prepared the manuscript.

Original Research Article

ABSTRACT

A simple version of the triangle model is proposed, that of a right triangle, which allows one to estimate from remote thermal/optical measurements the evapotranspiration fraction and surface soil moisture availability without reference to external variables even in the absence of a full range of vegetation cover and soil dryness. To date however, the triangle method has yet to be applied widely in the field, partly because of the triangle's limitations and partly due to its complexity whereby prospective users would be unequipped or unwilling to handle its technical aspects, including its mathematical requirements. After a brief description of the triangle geometry, the paper deals with current misconceptions in the use of the triangle/trapezoid method, including the way in which plants deal with water stress. The last part poses a scenario showing how the right triangle model could be applied easily and routinely at field level by the non-specialist.

1. INTRODUCTION

The so-called triangle method [1] identifies boundaries of a triangle or trapezoidal feature on a two-dimensional graph on which pixels of surface infrared temperature (Tir) are plotted versus a vegetation index (NDVI) or fractional vegetation cover (Fr). Boundaries of the geometric space of the pixel envelope define the interior values of evapotranspiration fraction EF (the ratio of evapotranspiration ET to net radiation Rn (minus the ground heat flux G)) and surface soil moisture availability (Mo), defined here as the ratio of soil water content to that at field capacity. Almost all versions of the triangle method assume linear variations of these quantities within the triangle borders. EF is generally favored over ET because it tends to remain approximately constant during the day. As such it is directly related to the Bowen ratio, the ratio of surface sensible heat flux H to ET.

Following the seminal article on the triangle method by Price.[2], at least 67 papers have been published up to the year 2022 (Fig. 1). Publications of these research papers began with those by American authors and were primarily built around the triangle model in which its boundaries were delineated visually. Subsequent publications introduced the concept of the trapezoid, a variant that was pursued by American, European, and Chinese authors; in many of these papers, the geometrical boundaries of the trapezoid were computed within a framework of mathematical/physical constraints [3]. Many later articles embraced both the triangle and trapezoid concepts using both visual and mathematical constructs to fix its boundaries [4].

Yet, despite the wealth of papers on this methodology, more needs to be achieved in applying it for specific purposes of monitoring soil water status. Several reasons exist for this oversight. This paper will address some of the problems and obstacles to making the triangle method a trusted operational tool. Rather than serve as a review of these many papers, after introducing some basic concepts and
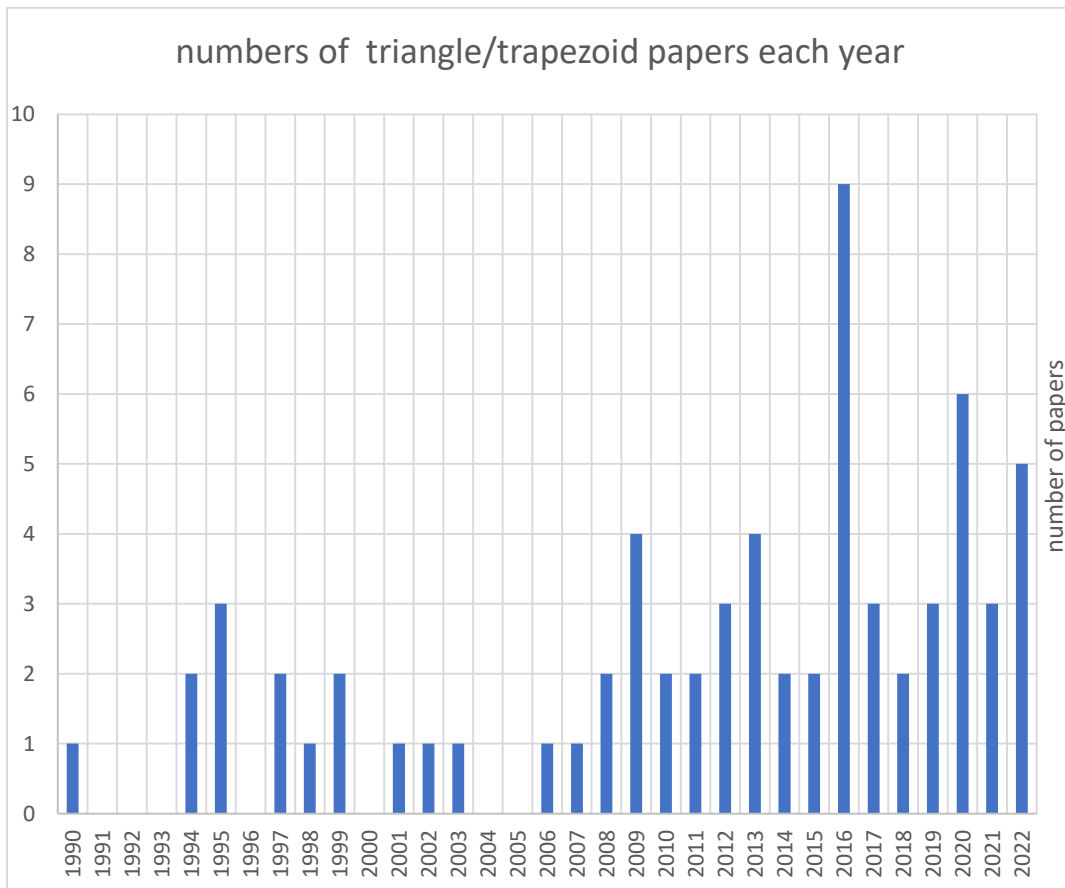

Fig. 1. Histogram of published papers directly referring to triangle/trapezoid models by year

the equations governing the triangle, this paper will briefly address both types of models (triangle and trapezoidal), including their limitations with emphasis on how plants respond to water stress. The goal of this paper is to offer a simpler and more practical version of the triangle method that avoids some of its deficiencies and misconceptions, while being more applicable to operational use by the intelligent but non-technical user. Next, it is explained how adding a time dimension to the triangle can provide further illumination on the progress of soil drying in a vegetated domain. Finally, its simplicity of use is demonstrated with a hypothetical scenario.

2. OVERVIEW OF THE TRIANGLE METHODS

2.1 The Right Triangle

Fig. 2 is a scatterplot of radiometric surface temperature (Tir) versus NDVI. Well known features of the scatterplot are the soil line, the limit of vegetation cover, the dry edge, the limit of surface soil dryness, and the moist (or cold) edge, which represents an upper limit of surface soil wetness. What is striking in this figure is the that these limits are so well-defined except perhaps for the moist edge; such sharply define boundaries strongly imply the presence of physical limits. These limits are zero (or some very small value) surface soil water content for the dry edge, zero plant cover for the soil line, and an upper limit of soil moisture, such as field capacity for the moist edge.

It is not a stretch of the imagination to view Fig. 2 as a right triangle, which is to say that the soil and moist edges are perpendicular to each other. Right triangles generally appear in NDVI/Tir coordinates when a full range of soil wetness and vegetation cover are present.

Only two anchor points (vertices) are needed to define a right triangle. One anchor point is at the vertex represented by the intersection of the soil line and the warm edge (the lower right-hand vertex in Fig. 2), where the minimum NDVI is defined as NDVIo, corresponding to bare soil, and the maximum Tir in the image (the same point) is defined as Tmax. This latter vertex point is referred to as (NDVIo/Tmax) which may be found over a dry, bare surface such as a parking lot, road, or dry beach sand [4]. The second anchor point is the intersection of the warm edge and the moist edge. At that point NDVIs is defined as the maximum vegetation cover corresponding to a fractional vegetation cover (Fr) of 1; the temperature at that point corresponds to the minimum Tir for the same point defined as Tmin. The latter may be found over sufficiently dense vegetation (such as a stand of trees); this vertex is referred to as (NDVIs/Tmin), the upper vertex in Fig. 2. These terms are defined mathematically in equations 1 and 2.

One method in assigning these so-called end members is visual, inspecting the scatterplot and identifying the edges by eye. Visually assigning edges to the scatterplot envelope depends on there being reasonably defined edges to the pattern and therefore enough pixels to form a recognizable pattern. Yet, even though [5] expresses grave reservations in the 'empirical' (visual) process of arbitrarily assigning the end members on a scatterplot, visual inspection may sometimes be superior to the more deterministic equations [6] which can engender a serious accumulation of errors that impact the value of the solution [7].

While visual delineation of a triangle on the scatterplot is admittedly subjective, dozens of examples of right triangles can be found in the scatterplots of many of the 68 papers referred to in Fig. 1 (e.g. [8], Fig. 2; [9], Fig. 11; [10], Fig. 6; [11], Fig. 5 and 6; [12], Fig. 2). [13–15] deliberately draw right triangles on their scatterplots, emphasizing that the moist edge must be a straight vertical line (in the coordinates of Fig. 2).

[16] show a scatterplot with a full range of pixels that conforms closely to a right triangle, similar to that in Fig. 2. [17] show that the dry edge closely fits a straight line in more than two dozen examples (their Fig. 6). Many of their scatterplots shown in their Fig. 5, shown without borders, could be drawn as right triangles. Moreover, some examples of scatterplots found in the literature in support of the trapezoid model, most of which determine the geometrical boundaries mathematically, can be redrawn with not much imagination as right triangles, such as Figs. 3a and b from [6,18] Moreover, those who favor the trapezoid model often adopt a right angle between the soil line and the warm edge ([19]; Fig. 2). The great advantage of a right triangle is that one need to specify only two anchor points to overcome the difficulty of triangle construction in the absence of a full range of vegetation cover and soil dryness. In so doing, the need to either visually or mathematically fix the triangle's boundaries is eliminated.
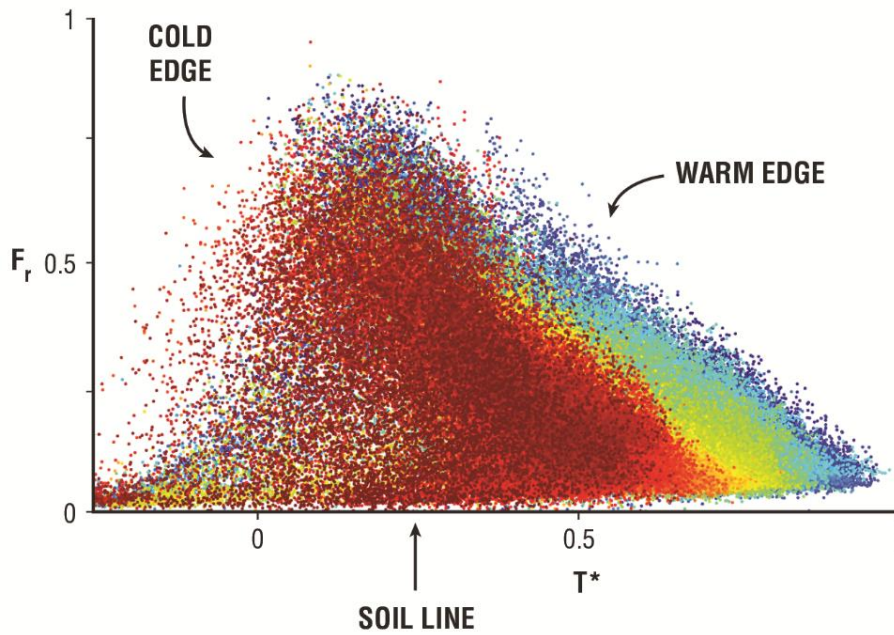
Fig. 2. Triangle created from Sentinel-3 image made over Spain at 1 km resolution plotted as a scatterplot of fractional vegetation cover Fr versus T*

Vertices A, B and C are referred to in the text, respectively, as NDVIo/Tmax, NDVIs/Tmin and NDVIo/Tmin. Salient features of the triangle are labeled. Colors represent pixel density, red being the most dense. Courtesy of George Petropoulos. Based on a figure from [20].

2.2 Theoretical Background

NDVI is scaled to fractional vegetation cover Fr, and Tir is scaled to a dimensionless temperature (T*), both of which vary from 0 to 1.

$$T^* = (Tir – Tmin) / (Tmax – Tmin) \qquad (1)$$

As defined in section 2.1, Tmin is the minimum surface infrared temperature for the image (at the location NDVIs), and Tmax, the maximum infrared temperature (at the location of NDVIo). T*, unlike Tir, is insensitive to daily variations in weather conditions.

Fr is defined as

$$Fr = ((NDVI – NDVIo) / (NDVIs – NDVIo))^n \qquad (2)$$

The exponent n is customarily taken as 2.0, although re-inspection of the original data for which this fit was made [21] suggests that n=1.6 would be a slightly closer fit.

T* along the warm edge is therefore

$$T^*(warm\ edge) = 1\text{-}Fr \qquad (3)$$

The moisture availability parameter is defined as

$$Mo = 1\text{-}[T^* (pixel)\ )/T^* (warm\ edge)] \qquad (4a)$$

Or, alternately.

$$Mo = 1\text{-}T^* (pixel)/(1\text{-}Fr) \qquad (4b)$$

Thus, Mo is zero along the dry edge and 1.0 along the wet edge, varying linearly between the warm and wet edges.

Evapotranspiration fraction is thus

$$EF = EF_s (1\text{-}Fr) + EF_{veg} *Fr \qquad (5a)$$

Here EF_s represents the evaporation fraction for bare soil, which is identical to Mo and EF_{veg} represents transpiration fraction for vegetation itself. Often, EF_{veg} is assumed as that at potential transpiration, which is not a bad assumption for vegetation that is not wilted; this quantity is therefore typically assigned a value of 1.0. Even well-watered vegetation, however, does not transpire freely as does bare, wet soil because of its stomatal resistance which impedes the transpiration to a degree that depends upon, among other things, on the plant species, its
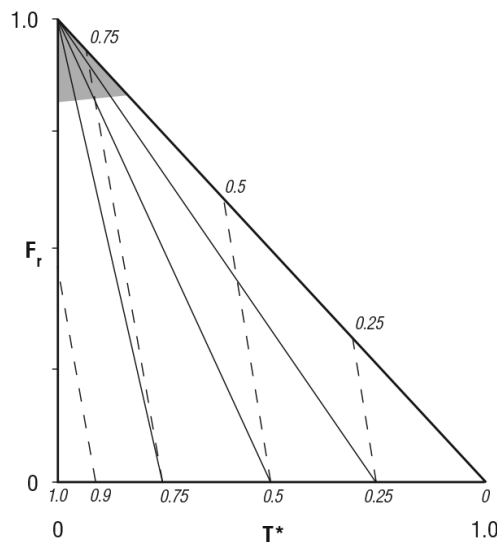
Fig. 3. Right triangle with isopleths of Mo (thin sloping lines leaning left and labeled below along the T* axis) and EF (dashed sloping lines labeled below and along the warm axis). The T* axis varies left to right from 0 to 1.0 (as labeled below the smaller numbers) and Fr varies from 0 to 1.0, bottom to top as labeled. Shaded area at the upper vertex represents part of the triangle that is lost when less than a full vegetation cover is chosen to represent a full canopy, that is when the value chosen for NDVIs is not the true value but corresponds to Fr<1. EF_{veg} was chosen as 0.8

previous stress, and root zone water availability. A more realistic value for EF_{veg}, allowing for a non-zero stomatal resistance, would perhaps be 0.8 Given this value for the transpiration fraction, equation 5a then becomes

$$EF = Mo(1-Fr) + 0.8Fr \qquad (5b)$$

Thus, to solve for Mo and EF within the triangle, all that is required are the two anchor points, and equations 4b and 5b. Given that the triangle is a right triangle, a template can be calculated from these two equations consisting of isopleths of Mo an EF within the triangle's borders. A solution to these two equations is shown in Fig. 3. It is customary to assume that these two parameters vary linearly across the triangle domain [22]. Of course, one is free to choose a value for EF_{veg} but this choice would not alter the form of equation 5b.[23]; see also [24] who present isopleths of the Priestly-Taylor coefficient (ϕ; essentially EF) that closely resemble the dashed lines for EF in Fig. 3.

3. RESULTS AND DISCUSSION

3.1 Triangle or Trapezoid

In addition to the triangle model, two types of trapezoid models have emerged in the literature:

the one phase and the two-phase models. These are now briefly presented.

3.1.1 The one phase trapezoid model

After the first volley of papers on the triangle method were published, most that followed during the years after 2000 described versions of the trapezoid. Adoption of the trapezoid model, rather than a triangle, was necessitated by the difficulty of specifying anchor points and the dry and warm edges in the absence of a full range of temperature and NDVI values. In the absence of a full range of vegetation fraction scatterplots tended to be truncated resembling a trapezoid, the outer borders of the non-shaded portion of Fig. 3.

Instead of relying on a visual fit, virtually all papers dealing with a trapezoid model determine the four end members deterministically with a set of equations based on both exact and semi-empirical relationships, such as the conservation of energy, the Priestly-Taylor equation, and equations governing surface fluxes. To solve these equations a variety of imperfectly known variables such as ambient temperature, surface albedo, surface emissivity, and canopy resistance. Implied in the latter is the concept of plant water stress and an indirect measure of the root zone water content.

3.1.2 The two-phase trapezoid model

Another approach to the trapezoid model attempts incorporates plant water stress by dividing the trapezoid into two triangles as shown in Fig. 4 [25–30].

The shaded portion represents the original triangle with the warm and moist edges. The unshaded part of the trapezoid represents a domain in which water stress is occurring in the plants with a depletion of water in the root zone and a progressive decrease in EF_{veg} from maximum at the warm edge for the soil, where the surface soil water content is zero, to a theoretical dry edge for vegetation where EF_{veg} (and therefore total EF) is zero.

The unshaded triangle in Fig. 4 represents a domain of stressed vegetation in which EF_{veg} decreases from a maximum (e.g., EF_{veg} = 1) at the soil warm edge (called the critical edge by Liu et al.[25]) to zero at the vegetation warm edge (called the dry edge by Liu et al. [25], which is not the same dry edge for soils. The dry edge for vegetation is a theoretical construct based on physical and mathematical formulations and does not seem to be found. A critique of this assumption within the context of actual plant behavior under stress is discussed in section 3.3.2.

3.2 Deficiencies in the trapezoid model

3.2.1 Triangle versus trapezoid

Simulations by Carlson et al.[31] and de Tomas et al.[9] show that the trapezoid appears in the scatterplot when the choice of maximum vegetation cover, NDVIs, does not correspond to a full vegetation cover Fr = 1. They show that when the leaf area index (LAI) is near or below 3, a portion of the upper vertex of the triangle (the shaded area in Fig. 3) is lost but when LAI is increased the trapezoid evolves to a full triangle. This is illustrated in Fig. 5 by showing that at LAI= 3, the maximum NDVI in the image does not adequately represent a full vegetation cover which is approximated by somewhat higher values of NDVI, the true value being at 0.8 in the figure. At increasing values of LAI, NDVI asymptotically approaches NDVIs, below which a trapezoid is likely to appear in the NDVI/Tir plot. Near or below LAI=3, the pixel distribution resembles a trapezoid because of openings in the vegetation cover. Thus, [19] adopt a trapezoid model, but most of their scatterplots

(their Fig. 9) pertain to values of LAI near or below 3. Introducing the trapezoid, therefore, adds unnecessary complexity to the problem of estimating Mo and EF and requires additional mathematical complexity, at least if its borders are to be determined objectively.

Choice of NDVIs when LAI is near or below 3 will yield a trapezoidal shape as in the unshaded part of the triangle in Fig. 4 (Based on simulations made by Carlson et al.[31] and de Tomas et al.[9]).

3.2.2 Plant water stress

A variety of models designed to fix the corner points of the trapezoid employ somewhat complex equations, many of which include plant canopy resistances, along with a number of other environmental variables. A canopy resistance implicitly assumes a dependence of the surface infrared temperature on root zone soil water content and therefore implicitly on a degree of crop water stress [4–6,25–30]. For both the simple trapezoid and the two-phase models, a canopy resistance thought to be appropriate to stressed vegetation is often assigned to the dry edge of the trapezoid, and weighted for Fr along the warm edge, so that overall canopy resistance varies along the dry edge and from dry to moist edges.

Inclusion of a second triangle within the trapezoidal framework (Fig. 4) is meant to accommodate pixels experiencing plant water stress, whereas the main (shaded) triangle corresponds to non-stressed vegetation. In this triangle, plant water stress increases from zero at the inner warm edge to a maximum at the outer warm edge.

However, this type of formulation is not correct. The problem of canopy resistance and crop water stress occurring as the result of a water deficit in the root zone is rather more complex than specifying a vegetation canopy resistance. Briefly, the process by which vegetation experience water stress is explained here as follows.

Plants become subject to water stress when the atmospheric demand for transpiration is more than can be supplied by the flow of water from the roots to the leaves. Plants respond to this by reducing the transpiration by means of increasing their stomatal resistance and their root and stem resistances. A reduction in transpiration will first

occur during the day when a critical point is reached, that is where atmospheric (including solar) demand begins to exceed the ability of the plant to provide the required amount of water from the roots. Plant type, age, physiology, and pre-existing water stress affect the time when increased stomatal resistance and reduced transpiration begins. Initially, this begins at the time of greatest atmospheric demand (solar noon) but on successive days the period of stress lengthens as long as demand for transpiration exceeds the ability of the plant to respond and meet the external demand. The period of transient demand over supply and its concomitant increase in stomatal resistance to accommodate this stress is referred to as 'mid-day stomatal closure', although the stomates do not close completely.

Increased stomatal resistance also raises the ensemble leaf temperature, though by an amount of no more than a few degrees or less, as suggested in Fig. 6. As root zone water is depleted over successive days without rainfall or irrigation, this transient phase of plant water stress lengthens and the effect on transpiration, leaf temperature, and carbon dioxide intake increases, flattening the transpiration curve but leaving these profiles unchanged before and after the stress period. Correspondingly, the bulk leaf temperature of the canopy becomes elevated during stressed conditions, as shown in Fig. 6 by the dotted and dashed lines. Accordingly, canopy temperature response to

increasing water stress and root zone water depletion lengthens on successive days. While the effects of water stress on transpiration tends to flatten the curve during the stress period, corresponding carbon dioxide profiles show a progressive depression and even a collapse during the stress period. These processes, described in detail by Lynn et al. [32] and Olioso et al. [33].

What is relevant to the triangle method is that plants respond to water stress is *transient* and the canopy temperature rise is constrained to just a few degrees C or less, even at solar noon; it is even smaller at the times of the polar orbital satellite overpass which can be an hour or more before solar noon (the vertical line in Fig. 6). Even when the period of water stress becomes acute, the plants never become hot like bare soil, but respond by curling their leaves, changing leaf orientation, or dropping them to the ground, thereby exposing the soil around the plants to direct sunlight and causing a decrease in NDVI. The result of this process therefore is a relatively small increase in ensemble radiative leaf temperature, an increase in bare soil temperature around the canopy, and a corresponding decrease in NDVI (Fr). Thus, changes in both NDVI and surface soil water content are both indicators of plant response to soil drying. It is indicative that, while [34] and [35] state that Tir is insensitive over dense vegetation, [36] find that NDVI alone may be a significant indicator of plant water stress.
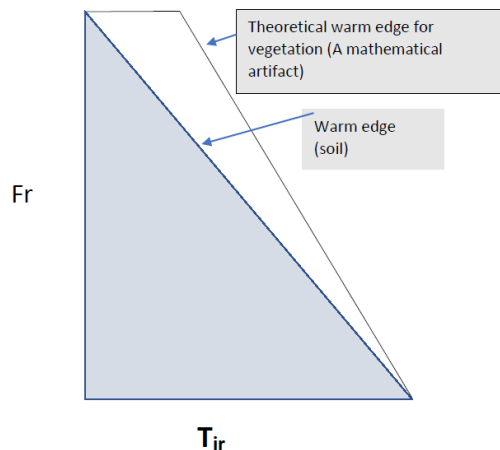
Fig. 4. Representation of the two-phase trapezoid. The shaded portion represents the original triangle with the warm and moist edges. The unshaded part of the trapezoid represents a domain in which water stress is occurring in the plants with a depletion of water in the root zone and a progressive decrease in EF_{veg} from maximum at the warm edge for the soil, where the surface soil water content is zero, to a theoretical dry edge for vegetation where EF_{veg} (and therefore total EF) is zero
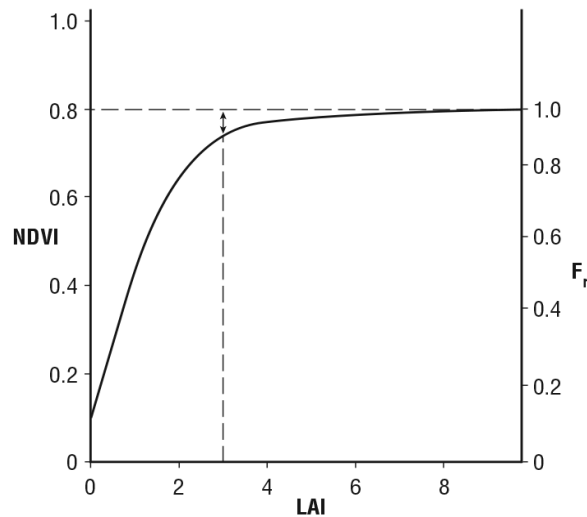
Fig. 5. A representation of simulations with a land surface model of NDVI versus leaf area index (LAI), showing that full vegetation cover (NDVIs; Fr = 1), approximated by the horizontal dashed line at NDVI=0.8, is obtainable for vegetation cover with an LAI larger than a value of about 3

Since the satellite-viewed radiometric surface temperature of an ensemble of vegetation rises by only couple degrees C or less at satellite overpass time, points within the triangle experiencing water stress may migrate toward both lower NDVI and higher T* while mostly remaining within the triangle. Thus, a pair of pixels representing stressed and non-stressed vegetation might be found side by side within the triangle space. That few points do move across the dry edge is the reason why that feature tends to remain sharply defined and linear.

An exception to this statement might occur near the vertex of the triangle (the point designated as NDVIs/Tmin) where small temperature changes of a pixel could propel it across the warm edge simply because isopleths of T* lie so close together (Fig. 3). This possibility was recognized by Mallick et al. [37] and Li et al. [22] who note that the spillage of stressed pixels over the warm edge near the vertex (NDVIs/Tmin) and presumably migrating into the unshaded triangle in Fig. 4 could create a scatterplot that indeed resembles a trapezoid. This possibility needs to be further investigated. It is also quite likely that pixels representing stressed vegetation are more likely to be found closer to the dry edge than pixels representing unstressed vegetation. This, too, is an idea that needs to be investigated further.

In sum, contrary to many statements made in the literature, at it is impossible to judge whether individual pixels within the triangle represent water stress or serve as reliable indicators of root zone water depletion (a situation recognized by Li et al. [22]). Thus, *no critical warm edge exists for plants as it does for soils, nor can the triangle capture root zone moisture or the state of plant water stress directly as claimed in many papers.* It is telling that writing of the two-phase model ([25], Fig. 7) and ([6], Fig. 1) show a scatter of points with almost none falling within the triangle corresponding to the 'unstressed' (shaded) triangle in Fig. 4.

Thin vertical line represents the time of a polar orbiting satellite overpass. Figure is based on simulations with a soil/plant/atmosphere model made by the author and described by Lynn et al., Olioso et al.[32,33], SR = sunrise; SN = solar noon; SS = sunset.

3.3 Agreement between Estimated and Measured Values of Soil Water Content and Ef

While all the papers published on the triangle method, in comparing their results with field measurements of soil water content and evapotranspiration, show modest agreement between measurements of EF and those estimated from the triangle method, estimates of root zone soil water content, however, are often poor for individual days when compared with field data for a single day (e.g.[36]). Many studies show some correlation between measured soil

water content and that obtained from the triangle method, but the correlation coefficients (R^2) while often moderately high for EF are typically small for soil water content [34], usually much less than 0.5. Much better correlations between estimated and measured soil water content are cited in the literature, but mostly where the numbers have been composited from several days of satellite and ground measurements, as in [21] and [38]. In these articles R^2 was quite high for data composited for an entire period, but nevertheless poor for individual days. Similar improvement when the data are composited was also found for EF [26,27] and for surface sensible heat flux [39].

Best agreement between estimated and in situ measurements seems to correspond with intermediate values of NDVI, but with improving agreement with decreasing NDVI. Poorest agreement sometimes occurs at the extremes of NDVI (or Fr) [40]. In areas with low Fr, agreement soil water measurements made over the top 5 cm or more, sometimes how poor agreement with those estimated remotely because the soil forms a dry surface crust over the top 1 - 2 cm trapping high soil water below due to the low hydraulic conductivity in the dry soil above [41,42]. [40], citing model results from other journal articles, show that, for thin, dry soils, EF can still become important because it depends more directly on the vegetation cover rather than soil water content. At high vegetation cover soil water content tends to be more evenly distributed with depth, which may be why [15] found some correlation between Tir and root zone soil water measurements at high NDVI. Generally, however, measurement noise tends to overwhelm the temperature signal at high NDVI because small errors in surface radiative temperature can result in serious errors in Mo where its isopleths lie close together in the triangle (Fig. 3) [12,37]. In sum, indirect root zone soil water content measurements using optical/thermal sensors are unreliable, but sometimes show reasonably good agreement for EF, and with measurements of soil water content in the time domain – that is, when individual daily measurements are combined over several days [43].

3.4 The Time Domain

Although individual points within the triangle are not necessarily reliable indicators of soil water content, compositing Mo and EF over a succession of images may constitute a more reliable indicator of plant water stress. The latter is manifested both by increases in surface infrared temperature (due, in part, to the increase in the amount of drying, bare soil visible to the radiometer) and decreases in NDVI (Fr) over several successive images. If axes of the right triangle are scaled identically, as shown in Fig. 7, congruent triangles can all be stacked vertically where the vertical axis represents times of successive triangles. A pixel representing a fixed location on the ground may move in triangle space with time. The schematic Fig. 7, representing of a series of three triangles on successive days, shows the pixel migrating toward lower Fr and higher T*, as would occur for situations involving increasing plant water stress, reflective of decreasing soil water content in the root zone. Successive points along the trajectories in three-dimensional space can be projected to a two-dimensional plane for easier visualization.

An analogous situation in which points within the triangle migrate toward the vertex (NDVIo/Tmax) occurs with urbanization. [44] show that over a 7-year period, pixels for San Jose', Costa Rica, migrated toward lower Fr and higher T* in response to progressive urbanization. Different neighborhoods exhibited different trajectories, but all showed movement toward the dry corner of the triangle where Fr=0 and T*=1. [45] (their Fig. 7b), looking at images over Sicily, showed points moving from near the vertex NDVIs/Tmin toward the soil line near the vertex NDVIo/Tmax with time.

4. THE RIGHT TRIANGLE METHOD

4.1 Requirements for its practical use in the field

No practical application of the triangle method can be successful unless it is simple and easy to apply by the non-specialist. It must not be dependent on solving mathematical equations or in laborious analysis procedures, including choosing its variables. [46] provide such a method for obtaining EF based on statistical analysis of the warm and cold edges. Here, as in [47], solution of the problem is reduced to obtaining two anchor points, where the focus is on both EF and soil water content, the latter being the more difficult of the two to resolve.
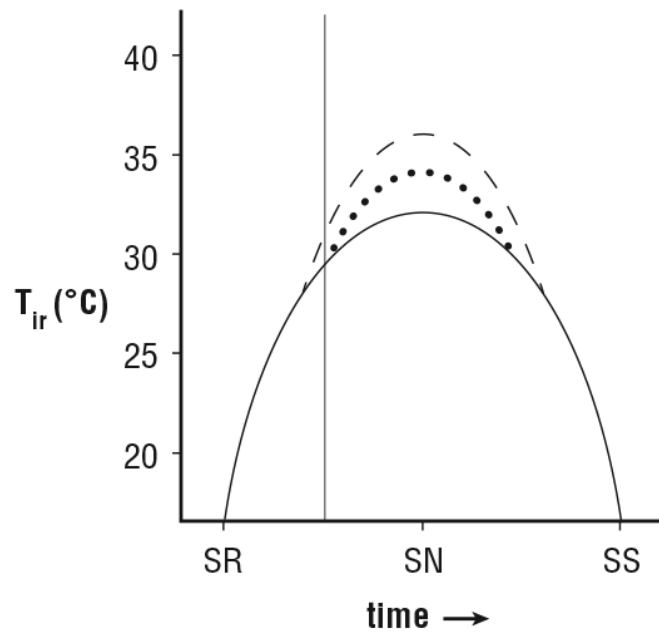
Fig. 6. Schematic depiction of the temperature curve for an ensemble of plants representative of typical row crops with time on successive days for unstressed soil moisture conditions (solid curve), moderately stressed conditions (dotted line) and severely stressed conditions (dashed line). SR refers to sunrise, SN to solar noon and SS to sunset. Thin vertical line represents the time of a polar orbiting satellite overpass. Figure is based on simulations with a soil/plant/atmosphere model made by the author and described by [32,33], SR = sunrise; SN = solar noon; SS = sunset
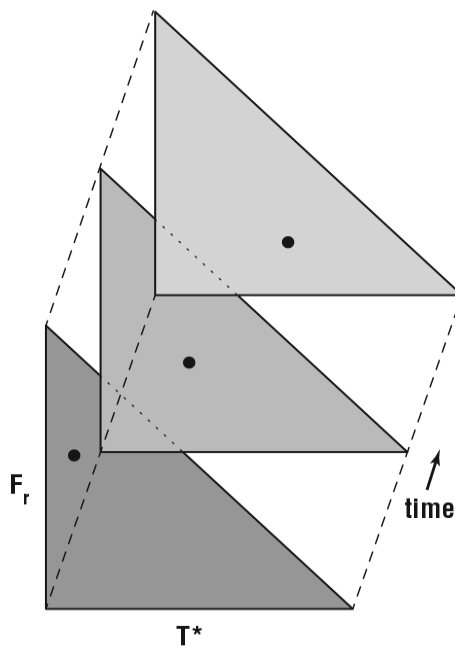
Fig. 7. Schematic representation of the three-dimensional triangle showing the location and movement in time of a pixel on three successive days at a fixed ground location (black dot)

4.2 Specifying the Two Anchor Points

All that is needed to estimate EF and Mo, therefore, is to specify two vertices of the triangle (NDVIo/Tmax) and (NDVIs/Tmin), To do this, one of two methods can be employed: (1) histograms of NDVI and Tir are created, outliers discarded, and the end points of these histograms equated with the desired four variable for the two corner points; (2) NDVIo/Tmax can be assigned to values appropriate to paved surfaces and end NDVIs/Tmin equated with the temperature over, a dense stand of trees. This assignment of end member points will be done in preprocessing mode by the computer or through a quick inspection of the temperature and NDVI image by the user. However, as pointed out by Tang et al. [46], care must be taken to avoid taking spurious end points. This can be avoided by making sure that both NDVI and T* are at the same locations in the image.

5. APPLICATION FOR THE NON—SPECIALIST: A SCENARIO

To be of practical use in assessing soil drying, points within the triangle must be followed in real time. Imagine an 'app' that would be able to create the right triangle and compute in real time its derived properties Mo and EF. Steps to accomplish this, similar to those described in a flow diagram by Singh et al. [48] (their Fig. 2), are now described.

In the present scenario, a non-specialist (farmer, watershed manager, city planner, etc.) desires to quickly know the water status of an area of interest (cropland, watershed, etc.). All that is needed for this user is to identify the domain of interest on a satellite image, a subset of the larger image. The only other task that the user would need to perform is to make any final adjustments as necessary at the end of the process,

5.1 Preprocessing Within the 'App'

First, the user downloads a satellite image (Sentinel 2, ECOSTRESS, MODIS, Landsat) centered on the area of interest but extending much beyond it. Then the smaller domain of interest (a field, watershed, etc.) is specified within the whole mage. The following steps are done automatically.

- Data from the image are downloaded: thermal infrared and visible radiances and land surface temperatures, and surface coordinates from the domain of interest, the latter being saved for future use. Cloud pixels and those for large bodies of standing water are removed. Procedures for making these adjustments to the image are simple but lie beyond the scope of this paper.
- Thermal infrared temperatures (Tir) and normalized difference vegetation index (NDVI) are calculated from these data.
- Histograms of Tir, NDVI, and other products as desired are created
- End member values of Tmax, Tmin, NDVIo and NDVIs are determined from histograms of Tir and NDVI or on inspection of the image as described in section 4.2. Outliers are first removed.
- Scatterplot of Tir/NDVI is created as on Fig. 8, along with two anchor points (the end members) drawn as small circles. If satisfied with the scatterplot, the user clicks on 'accept' wherein new scatterplot axes are created as T* and Fr (via equations 1 and 2) and the triangle is constructed, as on the right side of Fig. 8. Internal parameters Mo and EF are calculated using equations 4b and 5b.

5.2 Post Processing

- User inspects the plot and, if desired, adjusts the two anchor points by moving the small circles (anchor points) with the cursor, bearing in mind that the triangle should include as many points as possible, while maintaining its right triangle integrity with warm edge, moist edge and soil line adhering close to the pixel envelope. Each time an anchor point is moved the axes and interior values (Mo, EF) are recalculated.
- Once satisfied with the triangle, the user clicks on the button labeled 'done'. A new scatterplot is constructed using only pixels falling within the smaller domain of interest. Values of Mo and EF for this domain are stored for the smaller number of pixels within this scatterplot.
- Depending on the number of pixels within the smaller domain of interest, a single averaged value for each of these two variables is determined for the entire field or, if pixels are numerous, the user can specify averages to be taken over four quadrants of the domain or any other fractionation desired. Values of Mo and EF
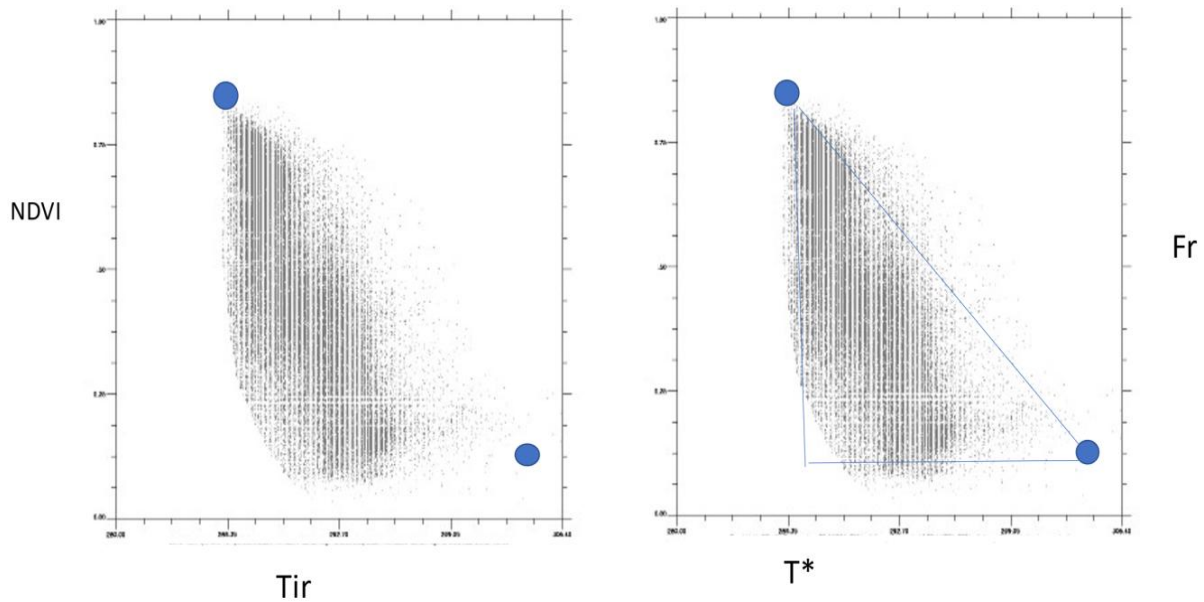
Fig. 8. ASTEr (90 m resolution) satellite image showing the basic image as pixels expressed in NDVI/Tir space (left) with the two anchor points shown as small, filled circles. The final image (right), expressed in Fr/T* space, shows the three critical edges of the triangle (those shown in Figure 2) drawn as straight lines. The purpose of this figure is to show that once two points in NDVI/ Tir space are identified and clicked on by the user, the complete solution for Mo and EF are instantaneously obtained

- and their geographical coordinates for these averaged values are printed out and stored.
- User can retrieve values of stored Mo and EF (and the coordinates of the domain of interest). These are plotted on a fresh set of coordinates of T* and Fr for the domain of interest, showing the trajectories of pixels with time, as in Fig. 7, but projected onto two-dimensional space for the domain of interest or for sub-sectors within the domain.

The final image (right), expressed in Fr/T* space, shows the three critical edges of the triangle (those shown in Fig. 2) drawn as straight lines. The purpose of this figure is to show that once two points in NDVI/ Tir space are identified and clicked on by the user, the complete solution for Mo and EF are instantaneously obtained.

6. FURTHER WORK

The right triangle model largely removes two obstacles to its practical application: (1) the problem of insufficient number of pixels to fill triangular space, and (2) the need to either visually or mathematically describe the triangle's boundaries. At present, an insurmountable problem remains, that of measurement frequency, which may be a problem for NDVI. As strongly suggested in this paper, NDVI may be as important a variable in diagnosing plant water stress as Tir. If the time domain offers the best opportunity to assess plant water stress, it is best that both Tir and NDVI be updated no more infrequently than every two or three days. At present, however, this is not the case.

What is further needed, if 33 years of research on the triangle method is not to have been in vain, is to develop simple operational procedures that can be applied by the non-technical user for immediate assessment of the soil water conditions in the field. What is no longer needed is to create more models and then to test them with field measurements. It is the opinion of this author that this approach has been sufficiently exploited.

Instead, it would be more useful for those involved in making the field measurements, those doing the image processing, and the modelers to work more closely together so as to explore at field level such issues as: (1) the relationship between the location of pixels within the triangle and the root zone soil water content (2) whether pixels located near the warm edge

represent points that are drier at root zone depth than pixels points along the moist edge; (3) whether pixels near the vertex (NDVIs/Tmin) spill over the warm edge and, if so, do these pixels represent plant water stress,

7. CONCLUSIONS

1. Aright triangle model greatly simplifies application of the triangle method.
2. Trapezoidal shapes may occur when the maximum NDVI (NDVIs) is not representative of a full vegetation canopy (Fr=1). This will occur when the LAI is around 3 or less.
3. It is virtually impossible to reliably determine root zone water content from a single image on a given day
4. It is virtually impossible to accurately assess from one image at a single time using thermal/optical measurements the degree of plant water stress for pixels within the triangular space.
5. Constructing an upper limit to plant stress, analogous to the dry edge, as in the two-phase method, is incompatible with the actual physiological way that plants respond to water stress.
6. Soil drying is accompanied by a progressive increase in surface radiant temperature (T*) and a decrease in NDVI (Fr)
7. Plant water stress should be more discernable by observing the trajectories of pixels within triangular space over time.
8. The triangle method will not be practical for application by users in the field unless the method is made simple, easy to apply, requires little or no technical or mathematical knowledge by the user, and images of NDVI and Tir are constructed at intervals no greater than 2 or 3 days. The present paper underscores the practicality of the right triangle method.
9. A schematic example is outlined, showing how the method could be easily and simply applied by a user.
10. Attention should now be focused on the relationship between the pixel's location within the triangle and root zone soil dryness.

ACKNOWLEDGEMENTS

COMPETING INTERESTS

Author has declared that no competing interests exist.

REFERENCES

1. Maltese A, Capodici F, Ciraolo G, LaLoggia G. Soil water content assessment: Critical issues concerning the operational application of the triangle method, Sensors.2015;15:6699-6718.
2. Price JC. Using special context in satellite data to infer regional scale evapotranspiration, IEEE Transactions Geoscience Remote Sensing.1990;28:940-948.
3. Zhao X, Liu Y, Peng J, Zhao D.: Evaluation of topography effect on evaporative fraction from MODIS data in Taihu Basin, China, 3rd International Conference on Biomedical Engineering and Informatics. Published by IEEE.; Accession Number 11662899, Yantai, China.2010.
   Available:
   https://doi.org/10.1109/BMEI.2010.5639357.
4. Zhang R, Tian J, Su H, Sun X, Chen S, Xia J. Two improvements of an operational two-layer model for terrestrial surface heat flux retrieval, Sensors.2008; 8:6663-6687.
5. Sun H, Wang Y, Liu W, Yuan S, Nie R, Comparison of three theoretical Methods for determining dry and wet edges of the LST/FVC space: Revisit of method physics, Remote Sensing. 2017;9,528.
6. Long D, V Singh, Scanlon B. Deriving theoretical boundaries to address scale dependencies of triangle models for evapotranspiration estimation, J. Geophysical Research. 2012;117.
7. Peng J, Liu Y, Zhao X , Loew A. Estimation of evapotranspiration from MODIS toa radiances in the Poyang Lake Basin, China, Hydrol. Earth Syst. Sci.2013;17:1431.
8. Jiang L, Islam, Estimation of surface evaporation map over southern Great Plains using remote sensing data, Water Resources Research. 2001;37:329-340.
9. de Tomas A, Nieto H, Guzinski R, Salas J, Sandholt I, Berliner P. Validation and scale dependencies of the triangle method for the evaporative fraction estimation over heterogeneous areas, Remote Sensing of Environment. 2014;152: 493-511.

10. Zhang H, Gorelick SM, Avisse N, Tilmant A, Rajsekhar D , Yoon J. A new temperature-vegetation triangle algorithm with variable edges (TAVE) for satellite-based actual evapotranspiration /estimation, Remote Sensing. 2016;8.

11. Silva-Fuzzo DF, Carlson TN, Kourgialas NN, Petropoulos GF, Coupling remote sensing with a water balance model for soybean yield predictions over large areas, Earth Science Informatics. 2019;13:345-359.

12. Kasim AA, Carlson TN, Lisman HS, Limitations in validating derived soil moisture content from thermal/optical measurements using the simplified triangle method, Remote Sensing. 2020;12: 1155.

13. Nguyen HH, Cho S, Choi M. Synergy of SAR and optical-thrmal infrared remote sensing for soil moisture estimation in agro-pastoral transitional zone, Ag. and Forest Meteorology. 2022;312, 108719.

14. Nishida K, Nemani RR, Glassy JM, Running SW. Development of an evapotranspiration index from Aqua/MODIS for monitoring surface moisture status, Trans on Geoscience and Remote Sensing. 2003;41:493-501.

15. Wang S, Garcia M, Ibrom A, Jakobsen J, Koppl CJ, Mallick K, Loomis MC, Bauer-Gottwein P. Mapping root-zone soil moisture using a temperature-vegetation-triangle approach with an Unmanned Aerial System: Incorporating surface roughness from structure and motion, Remote Sensing. 2018:10.

16. Batra N, Islam S, Venturini V, Bisht G, Jiang L. Estimation and comparison of evapotranspiration from MODIS and AVHRR sensors for clear sky days over the Southern Great Plains, Remote Sensing Environ. 2006;103:1-15.

17. Sandholt I, Rasmussen K, Andersen J. A simple interpretation of the surface temperature/vegetation index space for assessment of surface moisture status, Remote Sensing Environ. 2002;79: 213-224.

18. Long D, Singh VP. Assessing the impact of end-member selection on the accuracy of satellite-based spatial variability models for actual evaporation estimation, Water Resources Research. 2013;49: 2601-2618.

19. Yang Y, Sheng S.A hybrid dual-source scheme and trapezoid framework-based evapotranspiration model (HTEM) using satellite images: Algorithm and model test, J. Geosphys. Res. 2013;228: 2284-2300.

20. Carlson TN, A brief analysis of the triangle method and a proposal for its operational implementation, Remote Sensing, 2020;12.
Available:https://doi.org/10.3390/rs2223832.

21. Gillies RR, Carlson TN, Cui J, Kustas WP, Humes KS. A Verification of the 'Triangle' Method' for obtaining surface soil water content and energy fluxes from remote measurements of the normalized difference vegetation index (NDVI) and surface radiometric temperature. International Journal of Remote Sensing.1997;18: 3145–3166.

22. Li ZL, Tang R, Wan Z, Bi Y, Zhou C, Tang B, Yan G, Zhang X. A review of current methodologies for regional evapotranspiration estimation from remotely sensed data, Sensors. 2009; 9:3901-3853.

23. Stisen S, Sandholt I, Norgaard A, Fensholt R, Jensen KH. Combining the triangle method with thermal inertia to estimate regional evapotranspiration -- Applied to MSG-SEVIRI data in the Senegal River basin, Remote Sensing of Environment. 2008;112:1242-1255.

24. Shu Y, Stisen S, Jensen KH, Sandholt I. Estimation of regional evapotranspiration over North China Plain using geostationary satellite data, Int. J. Appl. Earth Observation and Geoinformation. 2011;13:192-206.

25. Liu M, Tang R, Li Z-L, DuanS, Gao M, Ziwei X. Separating soil evaporation from vegetation transpiration by remotely sensed one phase and two-phase trapezoids, Ag. and Forest Meteor. 2022;327:109215.

26. Long D, Singh VP, A modified surface energy balance for land (in SEBAL) based on a trapezoidal framework, Water Resources Research, 2012a;48:W02528.

27. Long D, Singh VP. A two-source trapezoid for evapotranspiration (TTIME) from satellite imagery, Remote Sensing of Environment. 2012b;121:370-388.

28. Sun H. A two-source model for estimating evaporative fraction (TMEF) coupling

Priestly Taylor formula and two-stage trapezoid, Remote Sensing. 2016a;8: 248.

29. Sun H. Two-stage trapezoid: A new interpretation of the land surface temperature and fractional coverage space, IEEE J. Sel. Top. Appl. Earth Obs. Remote Sensing. 2016b;9:336-346.

30. Tang R. Li ZL An end-member-based two-source approach for estimating land surface evapotranspiration from remote sensing data. IEEE Transactions on Geoscience and Remote Sensing, 2017;55(10):5818-5832.

31. Carlson TN, Ripley DA. On the relationship between NDVI, fractional vegetation cover and leaf area Index, Remote Sensing of Environment. 1997;62: 241–252.

32. Lynn BH, Carlson TN. Stomatal resistance model illustrating plant vs external control of transpiration, Ag. and Forest Meteor. 1990;52:5-43.

33. Olioso A, Carlson TN, Bresson N. Simulations of a diurnal transpiration and photosynthesis of a water stressed soybean crop, Ag. and Forest Meteor.1996;81: 41-59.

34. Piles M, Vali-Ilossera M, Corbella I, Panciera R, Rudiger C, Corbella YI, Panciera R, Rudiger C, Kerr Y, Walker J. Downscaling SMOS-derived soil moisture using MODIS visible/infrared data, IEEE Trans.on geosc. and remote sensing. 2011;49:3156-3166.

35. Amani M, Parsian S, MirMazloumi SM, Aieneh O. Two new soil moisture indices based on the NIR-red triangle space of Landsat 8 data, Int. J. Appl. Earth Obs. Geoinform. 2016;50:176-186.

36. Chandrasekar K, Srikanth P, Chakraborty A, Choudhary K, Ramana KV. Response of crop water indices to soil wetness and vegetation water content, Advances in Space Research. Available: https//doi.org/10.1016/j.asr.2022.11.019.

37. Mallick K, Bhattacharya BK,Patel NK. Estimating volumetric surface moisture content for cropped soils using a soil wetness index based on surface temperature and NDVI, Ag. And Forest Meteorology. 2009;149:1327-1342.

38. Sadeghi M, Babaeian E, Tuller M, Jones SB. The optical trapezoid model: A novel approach to remote sensing of soi moisture applied to Sentinel-2 and Landsat-8 observations, Remote Sensing of Environment. 2017;198:52-63.

39. Tang R, Z-L Li, Tang B. An application of the T-VI triangle method with enhanced edges determination for evapotranspiration estimation from MODIS data in arid and semi-arid regions. Remote Sensing of Environment. 2010;114:540-551.

40. Rahimimzadeh-Bajgiran P, Berg AA, Champagne C, Omasa K, Estimation of soil moisture using optical/thermal infrared remote sensing in the Canadian Prairies, ISPRS J. of Photogrammetry and Remote Sensing. 2013;83:94-103.

41. Capehart WJ, Carlson TN, Estimating near-surface soil moisture availability using a meteorologically driven soil water profile model, J. Hydro. 1994;160: 1-20.

42. Capehart WJ, Carlson TN, Decoupling of surface and near-surface soil water content: A remote sensing perspective, Water Resources Research, 1997;33: 1383-1395.

43. Wang W, Huang D, Wang XG, Liu YR, Zhou E. Estimation of soil moisture using trapezoidal relationship between remotely sensed land surface temperature and vegetation index, Hydrology and Earth System Sciences. 2011;15:1699-1712.

44. Carlson TN, Sanchez-Azofeifa GA. Satellite remote sensing of land use changes in and around San Jose' Costa Rica, Remote Sensing Environ. 1999; 70:247-256.

45. Minacapilli M, Consoli S, D. Vanella, G. Ciraolo, and A. Motisi, 2016: A time domain triangle method approach to estimate evapotranspiration: Application in a Mediterranean region using MODIS and MSG SEVIRI products, Remote Sensing Environ. 174 10-23.

46. Tang R, Li ZL, Liu M, Jiang Y, Peng Z. A moisture-based triangle approach for estimating surface evaporative fraction with time series of remotely sensed data, Remote Sensing of Environ. 2022;280:113-212.

47. Jiang L, Islam, A methodology for estimation of surface evapotranspiration over large areas using remote sensing observations, Geophys. Research Letters. 1999;26: 2773-2776.

48. Singh R, Srivastava PK, Petropoulos G, Shukla S, Prasad R. Improvement of the triangle method for soil moisture retrieval using ECOSTRESS and Sentinel-2: Results over a heterogeneous agricultural field in northern India, Water. 2022;14:31-79.

Peer-review history:
The peer review history for this paper can be accessed here:
https://www.sdiarticle5.com/review-history/104268